Electronic Supplementary Material (ESI) for Dalton Transactions.

Pyrazine-imide complexes: reversible redox and MOF building blocks

*Matthew G. Cowan, Reece G. Miller and Sally Brooker**

Electronic Supporting Information

Contents

1 Solubility of [M^{II}(dpzca)$_2$] complexes 2

2 Supplementary synthetic details 3

2.1 Attempted preparation of framework complexes 3

3 Crystallographic data 4

3.1 Crystallographic tables 4

3.2 Refinement details 6

3.2.1 Hdpzca 6

3.2.2 {[Co^{III}(dpzca)$_2$]BF_4}$_2$·5CH_3CN 7

3.2.3 [Cu^{II}(dpzca)$_2$] 7

3.2.4 [Cu^{II}(dpzca)(H_2O)$_3$]$_2$$SiF_6$·2$H_2O$ 7

3.2.5 {[Co^{III}(dpzca)$_2$Ag](NO_3)$_2$(H_2O)$_2$}$_\infty$ [3·2(H_2O)] 8

3.2.6 {([Ni^{II}(dpzca)$_2$$Ag^{I}_{½}$](½$NO_3$)(x$H_2O$}$_n$ [4·x(H_2O)] 8

3.3 Additional Structural Diagrams 9

4 Cyclic voltammetry Data 10

4.1 Cyclic voltammetry of [Fe^{II}(dpzca$_2$] 10

4.2 Cyclic voltammetry of [Ni^{II}(dpzca$_2$] 12

4.3 Cyclic voltammetry of [Cu^{II}(dpzca$_2$] 14

4.4 Cyclic voltammetry of [Zn^{II}(dpzca$_2$] 15

5 UV-Visible spectroscopy 16

5.1 UV-Visible spectrum of [Fe^{II}(dpzca)$_2$] 16

5.2 UV-Visible spectrum of [Cu^{II}(dpzca)$_2$] 16

5.3 UV-Visible spectrum of [Ni^{III}(dpzca)$_2$]$^+$ 17

6 Atom numbering for ^{1}H-NMR assignment 17

7 References 17

1 Solubility of [$M^{II}(dpzca)_2$] complexes

Solubility tests were performed at room temperature using small quantities of the powder material, suspending them in the appropriate solvent and sonication for several minutes. The results are summarised in tables S1 – S5.

	H_2O	CH_3OH	EtOH	DMF	CH_3CN	CH_2Cl_2	CH_3Cl	CH_3NO_2
Insoluble	X	X	X	X				
Partially Soluble					X	X	X	
Soluble								X

Table S1. The solubility of [$Fe^{II}(dpzca)_2$] at room temperature. X denotes the observed solubility. Partially soluble was defined as obtaining a coloured solution after filtering the suspension through a plug of cotton wool.

	H_2O	CH_3OH	EtOH	DMF	CH_3CN	CH_2Cl_2	CH_3Cl	CH_3NO_2
Insoluble		X	X		X	X		
Partially Soluble	X			X			X	
Soluble								X

Table S2. The solubility of [$Co^{II}(dpzca)_2$] at room temperature. X denotes the observed solubility. Partially soluble was defined as obtaining a coloured solution after filtering the suspension through a plug of cotton wool.

	H_2O	CH_3OH	EtOH	DMF	CH_3CN	CH_2Cl_2	CH_3Cl	CH_3NO_2
Insoluble	X	X	X					
Partially Soluble				X	X	X	X	
Soluble								X

Table S3. The solubility of [$Ni^{II}(dpzca)_2$] at room temperature. X denotes the observed solubility. Partially soluble was defined as obtaining a coloured solution after filtering the suspension through a plug of cotton wool.

	H_2O	CH_3OH	EtOH	DMF	CH_3CN	CH_2Cl_2	CH_3Cl	CH_3NO_2
Insoluble		X	X	X		X		
Partially Soluble					X		X	X
Soluble	X							

Table S4. The solubility of [$Cu^{II}(dpzca)_2$] at room temperature. X denotes the observed solubility. Partially soluble was defined as obtaining a coloured solution after filtering the suspension through a plug of cotton wool.

	H_2O	CH_3OH	EtOH	DMF	CH_3CN	CH_2Cl_2	CH_3Cl	CH_3NO_2
Insoluble	X	X	X			X	X	
Partially Soluble				X	X			X
Soluble								

Table S5. The solubility of [$Zn^{II}(dpzca)_2$] at room temperature. X denotes the observed solubility. Partially soluble was defined as obtaining a coloured solution after filtering the suspension through a plug of cotton wool.

2 Supplementary synthetic details

2.1 Attempted preparation of framework complexes

Given the two framework structures assembled from $[M(dpzca)_2]^{+/0}$ building blocks with M = Co^{III} or Co^{II} and Ni^{II} by using silver(I) linkers,[1] analogous reactions with silver(I) tetrafluoroborate were attempted for M = Fe^{II}, Cu^{II} and Zn^{II}. These attempts were carried out using the same synthetic method used to produce the reported pair of isostructural MOFs $\{[Co^{III}(dpzca)_2Ag](BF_4)_2(H_2O)_2\}_\infty$ and $\{[Ni^{II}(dpzca)_2Ag](BF_4)0.5(acetone)\}_\infty$. These were unsuccessful, but for completeness a few observations and comments follow.

The reaction with $[Fe^{II}(dpzca)_2]$ produced a brown *inhomogeneous* solid which was not characterised further. The easily accessible oxidation potential for this building block to $[Fe^{III}(dpzca)_2]^+$ (see manuscript, Table 1 and Figures 8 & 9) may be one of the factors complicating this reaction.

The reaction with $[Cu^{II}(dpzca)_2]$ produced a small amount of green microcrystalline solid which microanalysis showed to have very low carbon, hydrogen and nitrogen composition. The lack of framework formation in this case is attributed to the expected lability of $[Cu^{II}(dpzca)_2]$. It is also worth noting that, likely for the same reason, few examples of polymeric structures produced from the pyridyl analogue, $[Cu^{II}(bpca)_2]$, have been reported.[2]

The reaction with $[Zn^{II}(dpzca)_2]$ produced some crystals of a three-dimensional coordination polymer comprised only of silver(I) and pyrazine-2-carboxylic acid, $[Ag^{I}(C_5H_3N_2O_2)]_\infty$, the structure of which has already been reported in the literature.[3] This was not pursued further, but clearly at least some of the imide ligand has been cleaved to form the analogous carboxylic acid in the course of this reaction.

3 Crystallographic data

3.1 Crystallographic tables

Table S6. Crystal structure determination details for the Hdpzca ligand and the complex $[Co^{III}(dpzca)_2]BF_4 \cdot 5CH_3CN$.

	Hdpzca	**$\{[Co^{III}(dpzca)_2](BF_4)\} \cdot 5CH_3CN$**
Empirical formula	$C_{10}H_7N_5O_2$	$C_{50}H_{39}B_2Co_2F_8N_{25}O_8$
M_r	229.21	704.77
Crystal system	Monoclinic	Monoclinic
Space group	$P2_1/n$	$P2_1/c$
a [Å]	9.998(3)	12.4666(16)
b [Å]	6.8840(19)	29.676(4)
c [Å]	14.487(4)	16.9354(10)
α [°]	90	90
β [°]	95.037(13)	103.218(2)
γ [°]	90	93
V [Å^3]	993.2(5)	6099.4(12)
Z	4	8
T [K]	89(2)	93(2)
$\rho_{calcd.}$ [gcm^{-3}]	1.533	1.535
μ [mm^{-1}]	0.114	0.642
F(000)	472	2856
Crystal size [mm]	0.30 x 0.2 x 0.12	0.35 x 0.30 x 0.10
Θ range for data	2.82 to 26.58	1.37 to 25.35
Reflections collected	5966	64734
Independent reflections	3238	11134
R(int)	0.0465	0.0729
Max. and min.	0.9865 and 0.9667	0.9386 and 0.7492
Data/ restraints/	3059 / 0 / 155	11134 / 136 / 919
Goof (F^2)	0.914	1.044
R_1 [$I > 2\sigma(I)$]	0.0541	0.0651
wR_2 [$I > 2\sigma(I)$]	0.1389	0.1802
R_1 [all data]	0.1078	0.0939
wR_2 [all data]	0.1675	0.2040
Largest diff. peak and hole [eÅ^{-3}]	0.469 and -0.488	1.023 and -0.799

Table S7. Crystal structure determination details for [$\mathrm{Cu^{II}(dpzca)_2}$] and [$\mathrm{Cu^{II}(dpzca)(H_2O)_3]_2SiF_6\cdot 2H_2O}$.

	[$\mathrm{Cu^{II}(dpzca)_2}$]	**[$\mathrm{Cu^{II}(dpzca)(H_2O)_3]_2SiF_6\cdot 2H_2O}$**
Empirical formula	$C_{20}H_{12}Cu_1N_{10}O_4$	$C_{10}H_{16}Cu_1F_3N_5O_7Si_{0.5}$
M_r	519.95	452.86
Crystal system	Monoclinic	Triclinic
Space group	$P2_1/c$	P-1
a [Å]	8.8489(4)	6.5429(7)
b [Å]	27.4492(14)	8.1489(8)
c [Å]	8.5398(4)	15.3462(15)
α [°]	90	81.295(5)
β [°]	92.340(2)	85.364(6)
γ [°]	90	87.999(6)
V [Å^3]	2072.55(17)	805.94(14)
Z	4	2
T [K]	90(2)	89(2)
$\rho_{\mathrm{calcd.}}$ [gcm^{-3}]	1.666	1.866
μ [mm^{-1}]	1.108	1.474
F(000)	1052	460
Crystal size [mm]	0.50 x 0.30 x 0.14	0.2 x 0.2 x 0.06
Θ range for data collection [°]	1.48 to 26.38	1.35 to 26.48
Reflections collected	27699	32685
Independent reflections	4233	3314
R(int)	0.0415	0.0581
Max. and min. transmission	0.7454 and 0.5769	0.7454 and 0.6456
Data/ restraints/ parameters	4233 / 0 / 316	3314 / 15 / 268
Goof (F^2)	1.172	1.224
R_1 [$I > 2\sigma(I)$]	0.0366	0.0564
wR_2 [$I > 2\sigma(I)$]	0.0855	0.1184
R_1 [all data]	0.0402	0.0612
wR_2 [all data]	0.0871	0.1216
Largest diff. peak and hole [eÅ^{-3}]	0.460 and -0.443	0.934 and -0.674

Table S8. Crystal structure determination details for 3D MOF $\{[\mathrm{Co^{III}(dpzca)_2Ag](NO_3)_2(H_2O)_2}\}_n$ and 1D-chain $\{([\mathrm{Ni^{II}(dpzca)_2Ag^{I}_{½}](½NO_3)(xH_2O}\}_n$.

	$\{[\mathrm{Co^{III}(dpzca)_2Ag](NO_3)_2(H_2O)_2}\}_n$	**$\{([\mathrm{Ni^{II}(dpzca)_2Ag^{I}_{½}](½NO_3)(xH_2O}\}_n$**
Empirical formula	$C_{20}H_{16}AgCoN_{12}O_{12}$	$C_{20}H_{12}Ag_{0.5}N_{10.5}NiO_{5.5}$
M_r	783.25	600.05
Crystal system	Monoclinic	Monoclinic
Space group	$P2_1$/m	C2/m
a [Å]	9.3678(4)	14.619(3)
b [Å]	13.6094(6)	24.806(4)
c [Å]	10.1421(4)	9.861(4)
α [°]	90	90
β [°]	90.273(2)	122.003(7)
γ [°]	90	90
V [Å^3]	1293.00(9)	3032(1)
Z	2	4
T [K]	90(2)	90(2)
$\rho_{\mathrm{calcd.}}$ [gcm^{-3}]	2.012	1.314
μ [mm^{-1}]	1.490	0.999
F(000)	780	1204
Crystal size [mm]	0.2 x 0.1 x 0.1	0.2 x 0.1 x 0.1
Θ range for data collection [°]	2.01 to 26.40	2.96 to 26.51
Reflections collected	2145	28337
Independent reflections	811	3193
R(int)	0.1058	0.0860
Max. and min. transmission	0.862 and 0.836	22.839 and 2.2505
Data/ restraints/ parameters	2942 / 27 / 284	3193 / 7 / 177
Goof (F^2)	1.064	1.064
R_1 [I > 2σ(I)]	0.0547	0.0671
wR_2 [I > 2σ(I)]	0.1495	0.1807
R_1 [all data]	0.0687	0.0848
wR_2 [all data]	0.1596	0.1901
Largest diff. peak and hole [eÅ^{-3}]	1.187 and -1.249	1.020 and -2.465

3.2 Refinement details

3.2.1 Hdpzca

This structure was ‘de-twinned’ by Scott A. Cameron.

All non-hydrogen atoms were refined anisotropically and all hydrogen atoms were inserted at calculated positions and ride on the attached atom. No disorder. No solvent. Twin was identified by cellnow, which suggests twin domains are related by 180 degree rotation about real axis 1 0 0. Twinabs used for absorption correction, from which HKLF4 was made and used for space group assignment (XPREP) and initial structure solution (SHELXS). Twinabs also made an HKLF5 file (containing both twin domains) for use with final structure refinement. Averaged cell (and associated uncertainties) following integration were used for refinement. BASF parameter suggests equal proportion of each domain. Since the same reflection can be used for refinement of each domain the number of symmetry independent reflections is greater than the total number of reflections, giving a multitude of errors in CIFcheck.

3.2.2 $\{[Co^{III}(dpzca)_2]BF_4\}_2 \cdot 5CH_3CN$

The asymmetric unit contains $2\{[Co^{III}(dpzca)_2]BF_4\} \cdot 5CH_3CN$. All non-hydrogen atoms in the complexes are refined anisotropically. No disorder within the cationic complexes. C-H...O H-bonds and C...O pi-pi interaction present between adjacent complexes (shortest is 2.92A O7...C20'). The first BF_4^- was refined anisotropically and is well behaved. The second BF_4^- was modelled as a twirl disorder around B2-F21 and the SAME instruction was used to restrain the geometry. Disordered atoms were modelled isotropically. Further attempts to further model this as a twirl and inversion (0.5,0.3,0.2), did not improve values. 5 CH_3CN of crystallisation in the asymmetric unit: Two are full occupancy (N50,N60), 4(0.5; N80, N90, N96, N100), 2(0.25; N70, N75), 1(0.3; N110), 1(0.2; N115). Disordered, partial occupancy CH_3CN's lie in the same region of space: and the geometries were restrained using the SAME instruction to N50 (full occup). N70 and N75 MeCN share a common atom, C70:C76. N90 and N96 share a common atom, C91:C94. N110 and N115 share a common atom, C111:N115. The EXYZ & EADP instructions were used for these. PART instructions were used to separate the disordered positions. All acetonitrile molecules at less than half occupancy were modelled isotropically. H atoms were inserted at calculated positions and ride on the attached atom. The AFIX 33 command was used for some of the partial occupancy acetonitrile molecules.

3.2.3 $[Cu^{II}(dpzca)_2]$

$[Cu^{II}(dpzca)_2]$. Entire molecule in the asymmetric unit. Cu^{II} makes 2 long (trans) bonds to one ligand. No hydrogen bonds are suggested by HTAB. Pair of C11-H11···O1' and C12-H12···O1' bifurcated C-H···O H-bonds present between pairs of adjacent molecules (C11···O1' 2.98A; C12···O1 3.06A). All non-hydrogen atoms were refined anisotropically and all hydrogen atoms were inserted at calculated positions and ride on the attached atom. No disorder. No solvent.

3.2.4 $[Cu^{II}(dpzca)(H_2O)_3]_2SiF_6 \cdot 2H_2O$

1 complex, 3 waters and 1/2 SiF_6 in the asymmetric unit. Extensive hydrogen bonding network. Hydrogen atoms were generated from dummy atoms and placed using DANG and DFIX instructions with one exception. H41Y previously made an erroneous hydrogen bond to its symmetry equivalent, it was therefore located from the difference map, positioned using the HIMP instruction and fixed with the AFIX 1 instruction. DANG and DFIX instructions were used to restrain it's partner H41X. A B Alert is caused by close contact of H11X and H51X which is the result of hydrogen bonding between O11_H11X and O51.

3.2.5 {[Co^{III}(dpzca)$_2$Ag](NO$_3$)$_2$(H$_2$O)$_2$}$_\infty$ [3·2(H$_2$O)]

The data was de-twinned and processed using Cellnow and Twin Abs. HKLF 4 was used to generate the solution, then HKLF 5 was used for the refinement. The BASF parameter suggests it is a twinned crystal with approximately a 2/3:1/3 ratio of domains. Since the same reflection can be used for refinement of each domain the number of symmetry independent reflections is greater than the total number of reflections, giving a multitude of errors in CIFcheck, as expected. Half of the formula is in the asymmetric unit. All non-hydrogen atoms were refined anisotropically. All hydrogen atoms in the main residue were inserted at calculated positions and ride on the attached atom. Hydrogen atoms on the solvent water molecules were generated from dummy atoms and geometries idealised using DFIX 0.85 (0.02) and DANG 1.39 (0.04) instructions before being fixed in place using the AFIX 1 instruction. The nitrate anions are disordered over two parts, each of half occupancy.

3.2.6 {([Ni^{II}(dpzca)$_2$Ag$^{I}_{½}$](½NO$_3$)(xH$_2$O}$_n$ [4·x(H$_2$O)]

This 1D-chain polymer, {([Ni^{II}(dpzca)$_2$Ag$^{I}_{½}$](½NO$_3$)(approx. 5H$_2$O}$_n$, crystallises with a half occupancy nickel centre, one full occupancy imide ligand, and a quarter occupancy AgNO$_3$ in the asymmetric unit. Each nitrate anion is disordered over four quarter occupancy positions (forming two flat hexagons that share 1 side) and so was modelled isotropically - FLAT and SADI (to restrain N-O bond lengths and O···O separations) restraints were also applied in order to control the geometry. All other non-hydrogen atoms were refined anisotropically. The disordered solvent could not be successfully modelled so this electron density was instead dealt with by the SQUEEZE routine of PLATON,[4] which indicated that these molecules were equivalent to 25 electons (equivalent to 2.5 water molecules) per asymmetric unit (or 5 water molecules per Ni, x ≈ 5).

Geometry details

Table S9. Selected bond lengths and angles for Hdpzca and $[Cu^{II}(dpzca)(H_2O)_3]_2SiF_6·2H_2O$.

Parameter	**Hdpzca**	**$[Cu^{II}(dpzca)(H_2O)_3]_2SiF_6·2H_2O$.**
M-N_{pz}		2.005(4), 2.003(4)
M-N_{imide}		1.936(4)
M-OH_2		1.958(2), 2.322(2)
N_{pz}-M-N_{imide}		82.34(9)
N_{pz}-M-N_{pz}		161.74(9)
N_{imide}-M-OH_2		O11 1.949(3) O12 2.332(4) O31 2.660(3)
O_{imide} out of N_3 plane[b]	O1 0.0067 O2 0.0068	O1 -0.206(9); O2 -0.148(9)
Intra-ligand Centroid$_{OO}$···M···$N_{pz'}$[c]	90.3, 89.93[a]	77.7, 77.4
Intra-ligand $N_{pz'}$···M···$N_{pz'}$	111.93, 111.95[a]	154.93(7)
Distortion parameter[e]		Σ = 56.1, T = 0.79

[a] H3x was used as the central pivot due to the absence of a coordinated metal ion; [b] The plane is defined by the coordinated N_3 donor set of the same ligand; [c] centroid of the oxygen imide atoms; [d] pz and pz' refer to the coordinated and 'spare' pyrazine donors respectively; [e] calculated as described in the following references T,[5] Σ.[6]

3.3 Additional Structural Diagrams

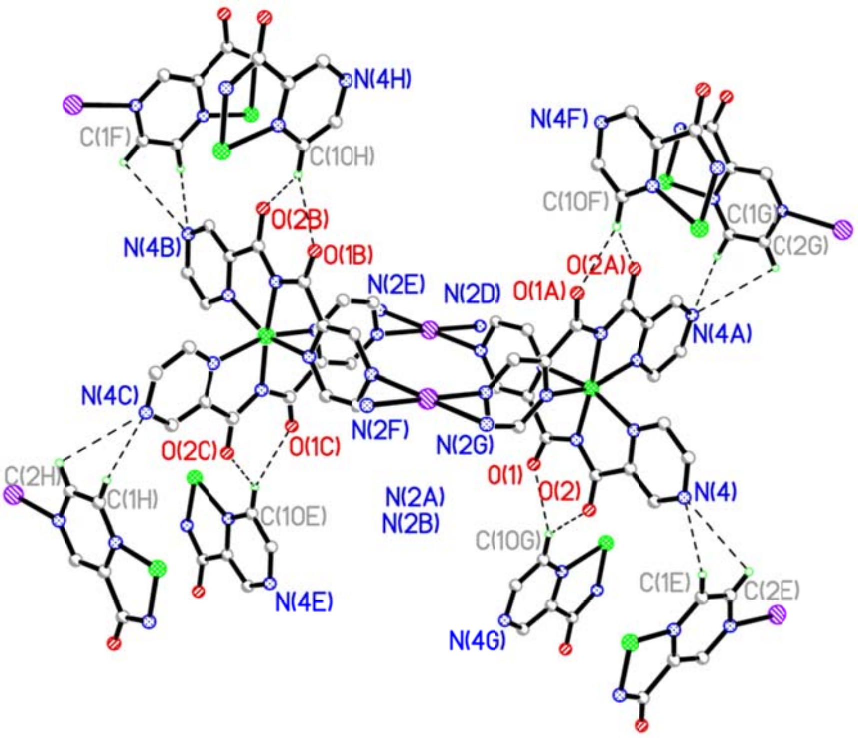

Figure S1. Inter-chain H-bonding interactions in the 1D chain, **4**, where the central molecule acts as an acceptor. Note that these interactions are reciprocated so that C1, C2 and C10 on the central molecule also act as H-bond donors.

4 Cyclic voltammetry Data

4.1 Cyclic voltammetry of [Fe^{II}(dpzca$_2$]

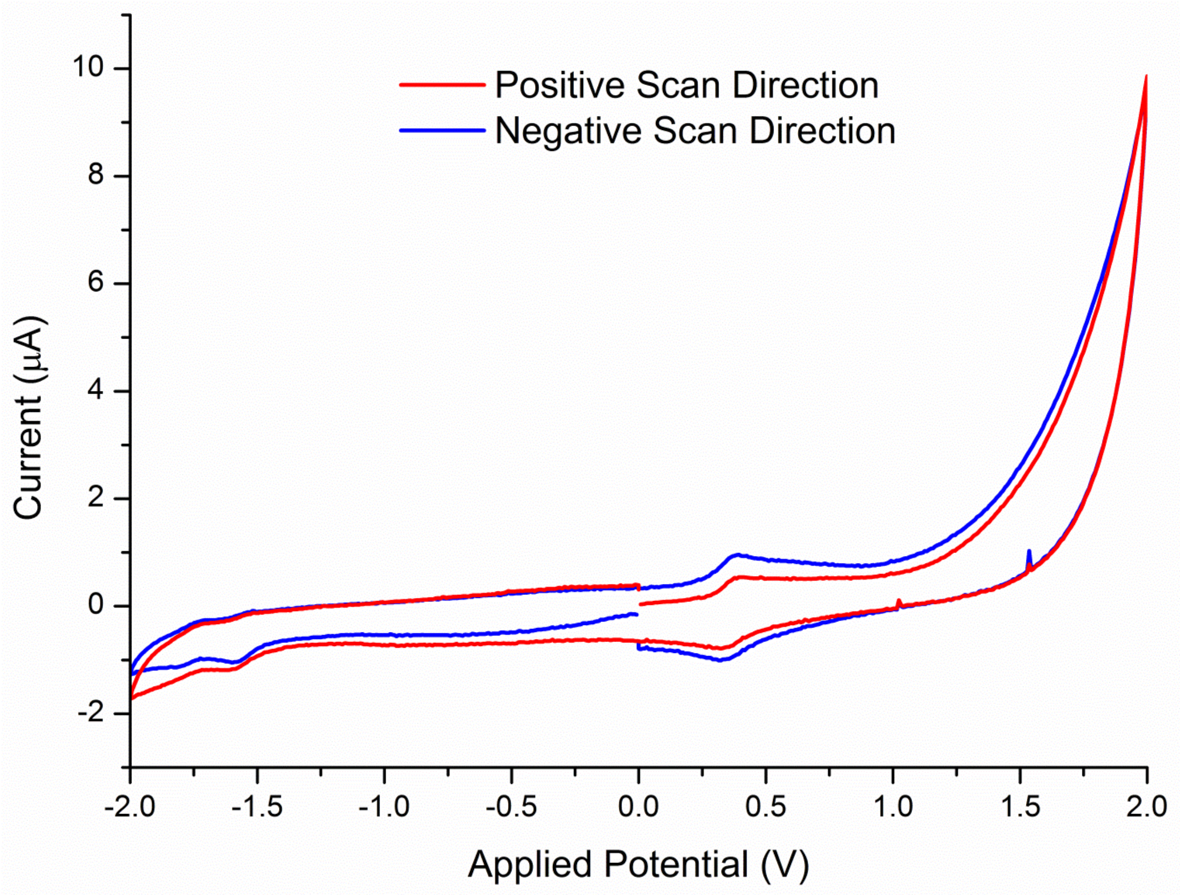

Figure S4. Cyclic voltammetry of a 0.449 mol L^{-1} suspension of [Fe^{II}(dpzca)$_2$] in acetonitrile **before** bulk electrolysis. Scan rate 200 mVs^{-1}. Ref 0.01 M AgNO$_3$/Ag.

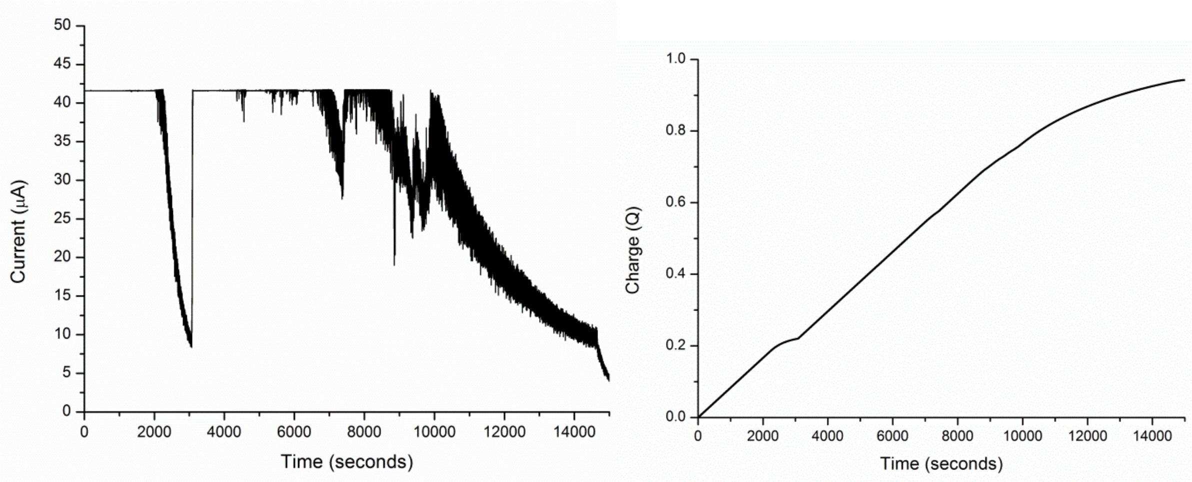

Figure S5. Bulk electrolysis of a 10 mL suspension of 0.518 mmol [Fe^{II}(dpzca)$_2$] in acetonitrile at 0.65 V passed 0.94 electron equivalents. Ref 0.01 M AgNO$_3$/Ag. The observed drops in current are due to settling of the suspended solid to the bottom of the cell, re-suspension of the solid resulted in restoration of the current.

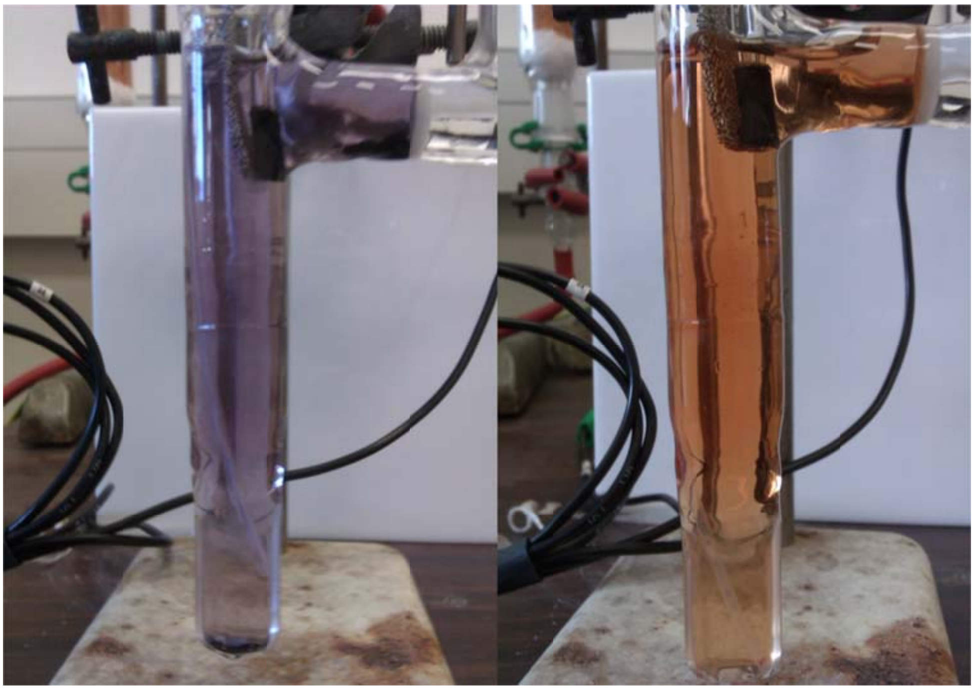

Figure S6. The reversible colour change observed during the oxidation of $[Fe^{II}(dpzca)_2]$ (left) to $[Fe^{III}(dpzca)_2]^+$ (right). Controlled potential electrolysis was performed at 0.65 V vs 0.01 M $AgNO_3/Ag$, on 10 mL of a 0.518 mmol L^{-1} suspension of $[Fe^{II}(dpzca)_2]$ in acetonitrile, resulting in the transfer of 0.94 electron equivalents.

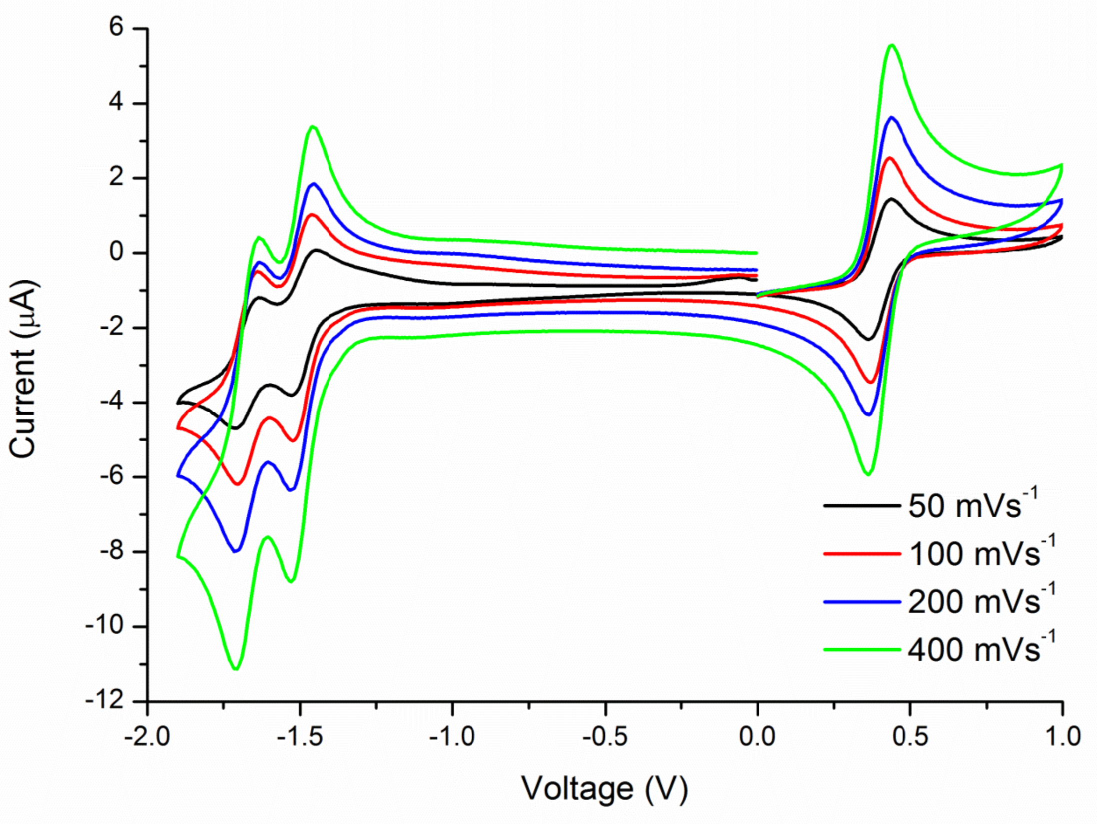

Figure S7. Scan rate study of a 0.518 mmol L^{-1} suspension of $[Fe^{III}(dpzca)_2]^+$ in acetonitrile **after** bulk electrolysis at 0.65 V which passed 0.94 electron equivalents. Ref 0.01 M $AgNO_3/Ag$.

4.2 Cyclic voltammetry of [$\mathrm{Ni^{II}}$(dpzca$_2$]

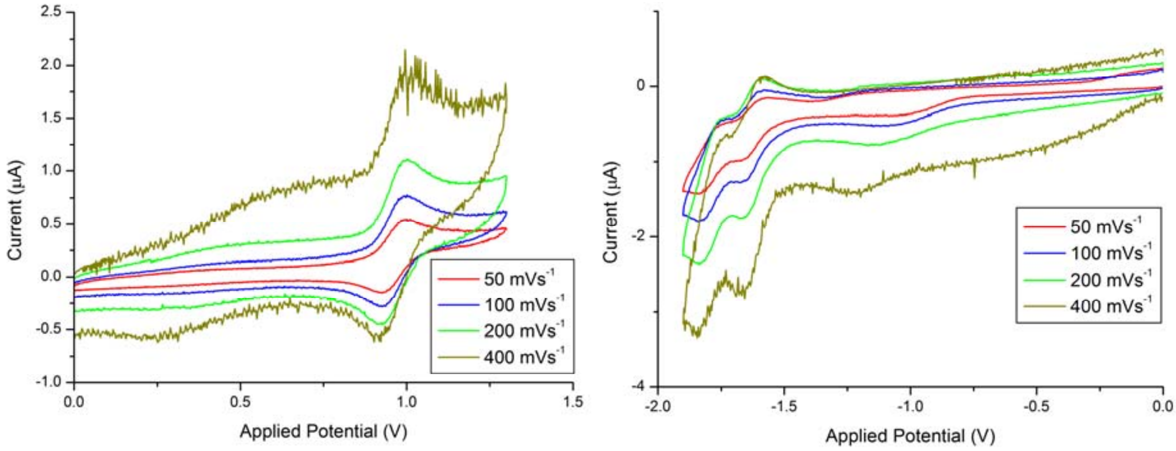

Figure S8. Scan rate studies of the metal based process (left) and ligand based processes (right) of a 1.1 mol L^{-1} [$\mathrm{Ni^{II}}$(dpzca)$_2$] suspension in acetonitrile. Ref 0.01 M $AgNO_3$/Ag.

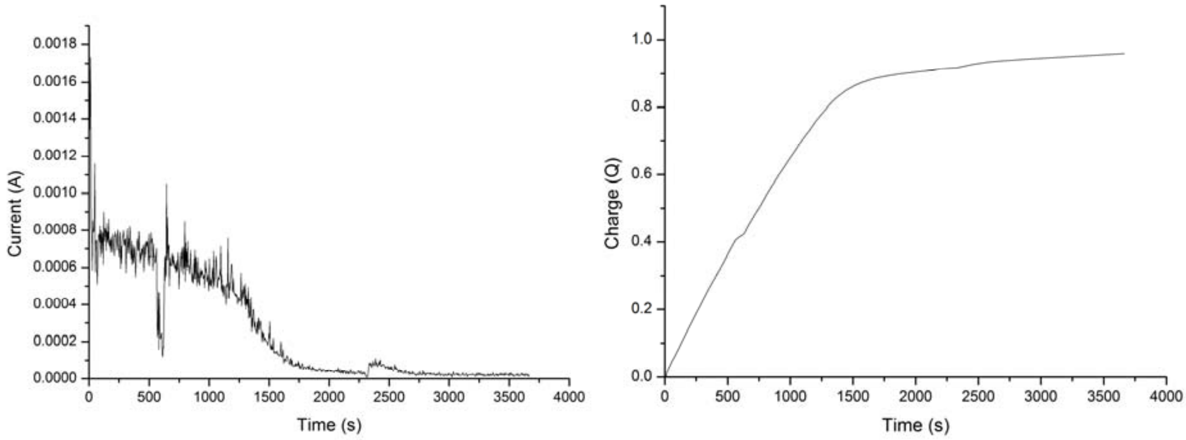

Figure S9. Bulk electrolysis of a 1.1 mmol L^{-1} suspension of [$\mathrm{Ni^{II}}$(dpzca)$_2$] in acetonitrile at 1.1 V passed 0.95 electron equivalents. Ref 0.01 M $AgNO_3$/Ag.

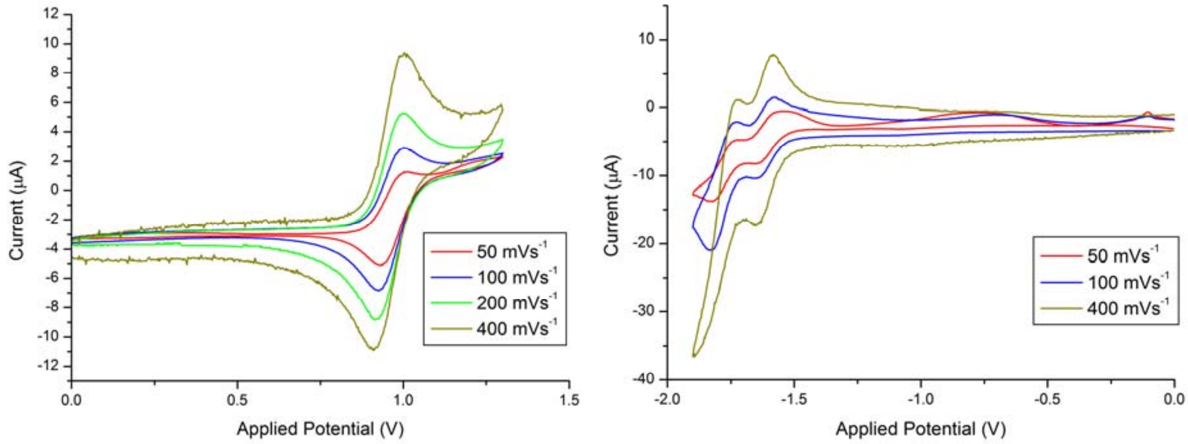

Figure S10. Scan rate studies of the metal based process (left) and ligand based processes (right) of a 1.1 mmol L^{-1} solution of [$\mathrm{Ni^{III}}$(dpzca)$_2$]$^+$ in acetonitrile **after** bulk electrolysis of a 1.1 mmol L^{-1} suspension of [$\mathrm{Ni^{II}}$(dpzca)$_2$] in acetonitrile at 1.1 V passed 0.95 electron equivalents. Ref 0.01 M $AgNO_3$/Ag.

Figure S11. The reversible colour change observed during the oxidation of [Ni^{II}(dpzca)$_2$] (left) to [Ni^{III}(dpzca)$_2$]$^+$ (right). Controlled potential electrolysis was performed at 1.1 V vs 0.01 M AgNO$_3$/Ag, on 10 mL of a 1.1 mmol L^{-1} suspension of [Ni^{II}(dpzca)$_2$] in acetonitrile, resulting in the transfer of 0.95 electron equivalents.

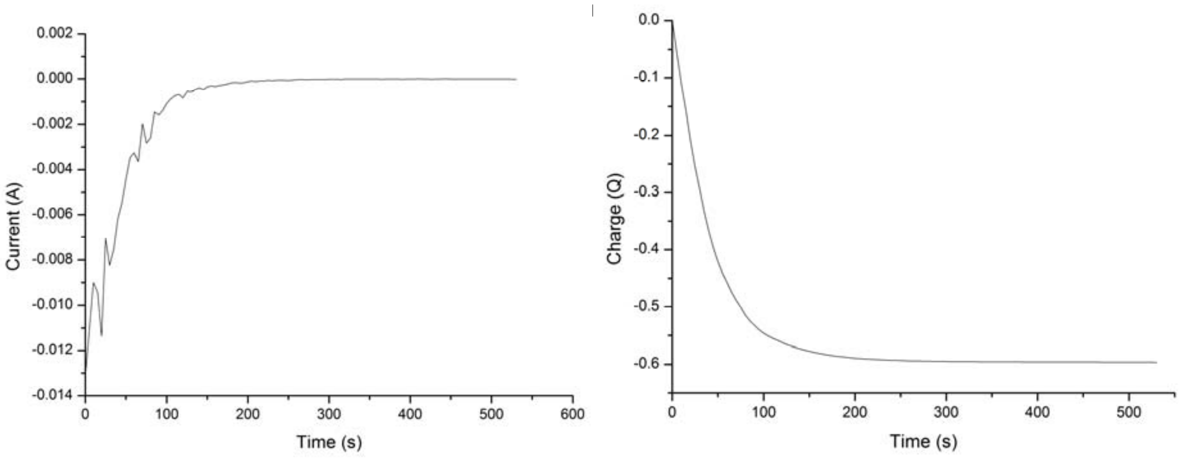

Figure S12. Bulk electrolysis of a 10 mL, 1.1 mmol L^{-1} solution of [Ni^{III}(dpzca)$_2$]$^+$ in acetonitrile at 0 V which passed 0.58 electron equivalents. Ref 0.01 M AgNO$_3$/Ag.

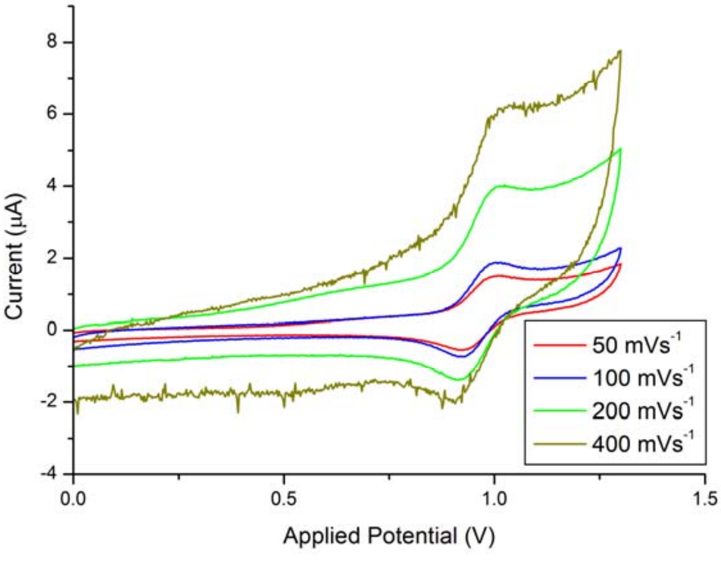

Figure S13. Scan rate studies of the metal based process of a 1.1 mmol L^{-1} suspension of [Ni^{II}(dpzca)$_2$] in acetonitrile **after** bulk electrolysis of a solution of [Ni^{III}(dpzca)$_2$]$^+$ at 0 V passed 0.58 electron equivalents. Ref 0.01 M AgNO$_3$/Ag.

4.3 Cyclic voltammetry of [Cu^{II}(dpzca$_2$]

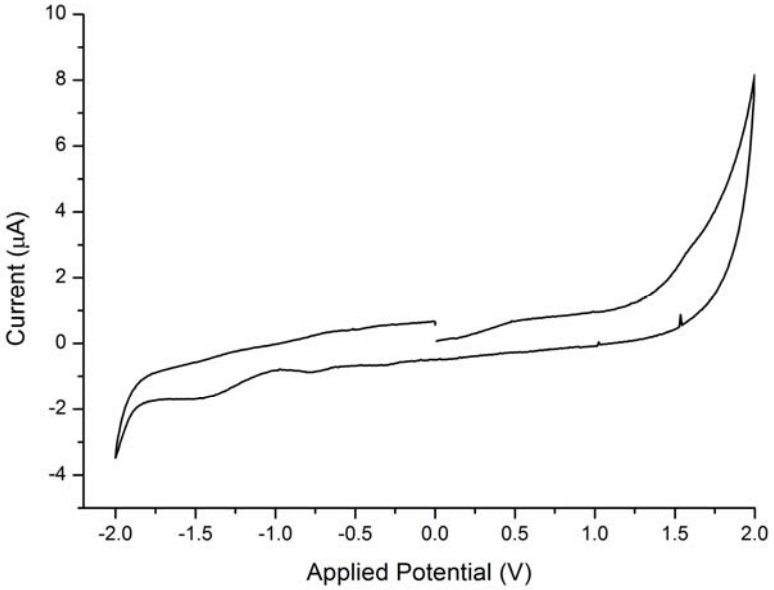

Figure S14. Full scan of a suspension of a 1.1 mmol L^{-1} suspension of [Cu^{II}(dpzca)$_2$] in acetonitrile starting at zero and going toward positive potentials. Scan rate 200 mVs^{-1}, ref 0.01 M AgNO$_3$/Ag.

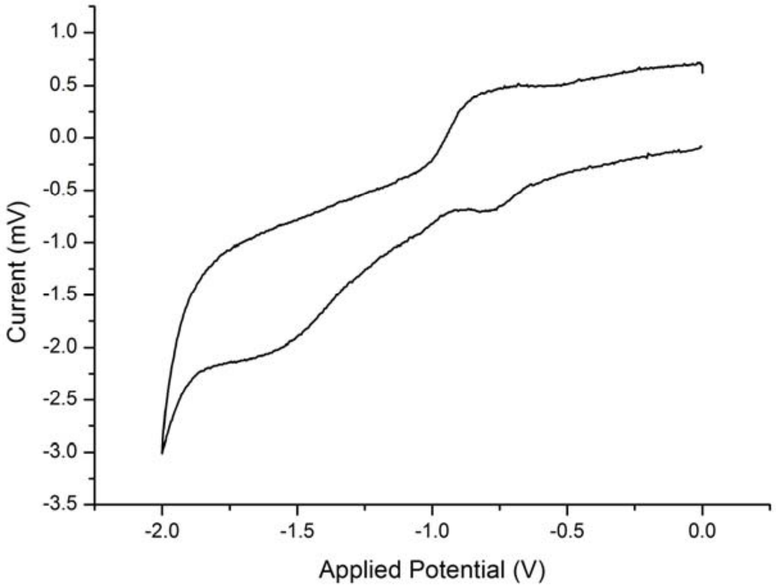

Figure S15. The cyclic voltammetry showing the reduction process of a 1.1 mmol L^{-1} suspension of [Cu^{II}(dpzca)$_2$] in acetonitrile starting at zero and going toward positive potentials. Scan rate 200 mVs^{-1}, ref 0.01 M AgNO$_3$/Ag.

4.4 Cyclic voltammetry of [Zn^{II}(dpzca$_2$]

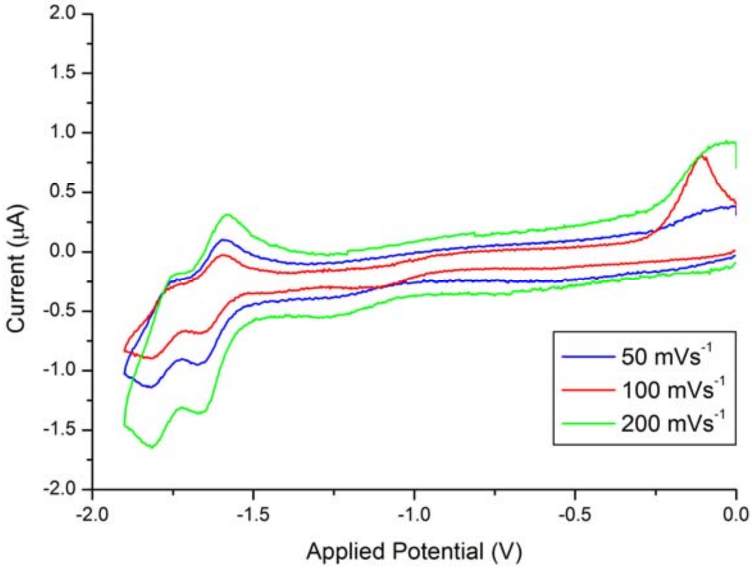

Figure S16. Scan rate study of a 1.2 mmol L^{-1} suspension [Zn^{II}(dpzca)$_2$] in acetonitrile starting at zero and going toward negative potentials. Ref 0.01 mol L^{-1} AgNO$_3$/Ag. Note that the scan rate of 400 mVs^{-1} has been omitted due to the low quality of the data.

5 UV-Visible spectroscopy

5.1 UV-Visible spectrum of [Fe^{II}(dpzca)$_2$]

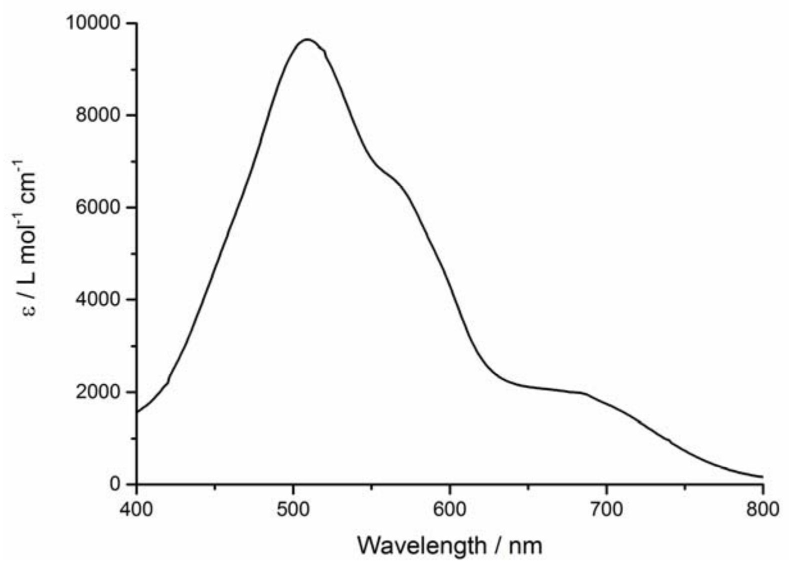

Figure S17. UV-Visible spectrum of [Fe(dpzca)$_2$] recorded in nitromethane. Absorbtions are observed at λ = 514, 567 and 690 nm with extinction coefficients; $\varepsilon_{514} = 9636$, $\varepsilon_{567} = 6568$, $\varepsilon_{690} = 1920$ L cm^{-1} mol^{-1}.

5.2 UV-Visible spectrum of [Cu^{II}(dpzca)$_2$]

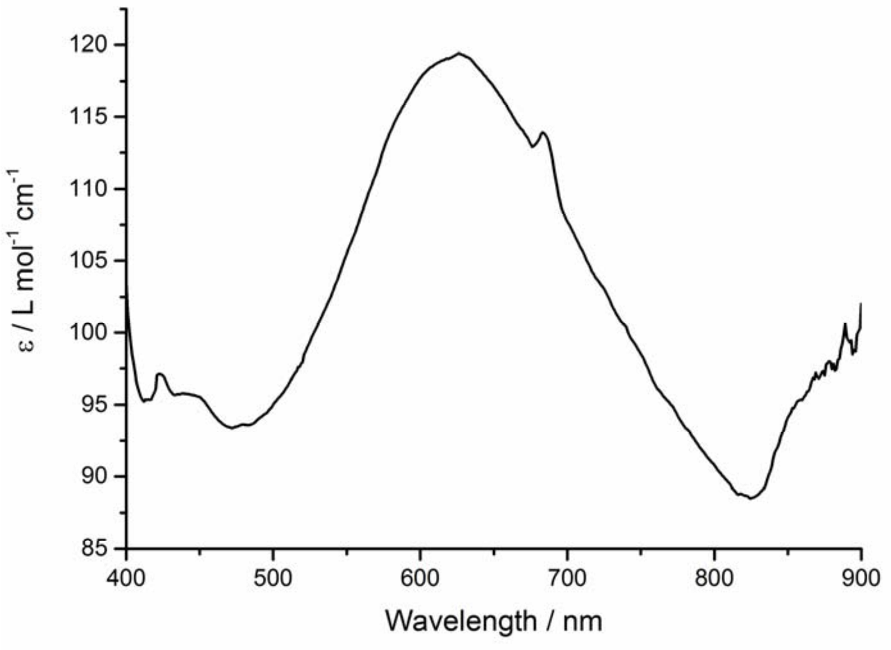

Figure S18. UV-Visible spectrum of [Cu^{II}(dpzca)$_2$] recorded in water. Major absorbtions are observed at λ = 654, 278 and $\varepsilon_{654} = 133$; $\varepsilon_{278} = 15{,}472$; $\varepsilon_{208} = 16{,}554$ dm^{3}cm^{-1}mol^{-1}.

5.3 UV-Visible spectrum of $[Ni^{III}(dpzca)_2]^+$

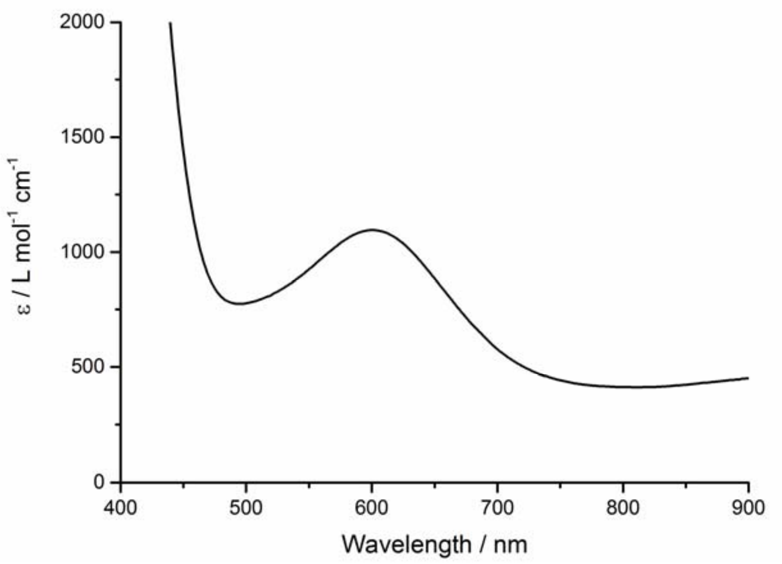

Figure S19. UV-Visible spectrum of $[Ni^{III}(dpzca)_2]^+$ in CH_3CN containing 0.1 equivalents $^tBu_4NPF_6$ (following bulk electrolysis at 1.1 V passed 0.95 electron equivalents) λ_{max} = 600 nm, ε_{600} = 1095 L cm^{-1} mol^{-1}.

6 Atom numbering for ^{1}H-NMR assignment

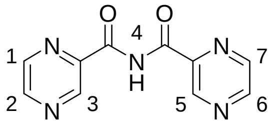

Figure S20. The ligand Hdpzca with the atom numbers used for hydrogen assignments.

7 References

1 M. G. Cowan, R. G. Miller, P. D. Southon, J. R. Price, O. Yazaydin, J. R. Lane, C. J. Kepert and S. Brooker, *Inorg. Chem.*, doi.org/10.1021/ic501876m.

2 M. G. Cowan and S. Brooker, *Coord. Chem. Rev.*, 2012, **256**, 2944.

3 F. Jaber, F. Charbonnier and R. Faure, *J. Chem. Crystallogr.*, 1994, **24**, 681; S. Qin, S. Lu, Y. Ke, J. R. Li, X. Wu and W. Du, *Solid State Sci.*, 2004, **6**, 753.

4 P. van der Sluis and A. L. Spek, *Acta Crystallogr., Section A*, 1990, **A46**, 194.

5 A. B. P. Lever, 'Studies in Physical and Theoretical Chemistry 33: Inorganic Electronic Spectroscopy', Elsevier, 1997.

6 M. G. B. Drew, C. J. Harding, V. McKee, G. G. Morgan and J. Nelson, *J. Chem. Soc., Chem. Commun.*, 1995, 1035.